Dual bioluminescence and near-infrared fluorescence monitoring to evaluate spherical nucleic acid nanoconjugate activity in vivo

Timothy L. Sita[a,b,c,d], Fotini M. Kouri[a,b], Lisa A. Hurley[a,b], Timothy J. Merkel[b,c], Alexandra Chalastanis[a,b], Jasmine L. May[a,b], Serena T. Ghelfi[a,b], Lisa E. Cole[b,c], Thomas C. Cayton[a], Stacey N. Barnaby[b,c], Anthony J. Sprangers[b,c], Nikunjkumar Savalia[b,c], Charles David James[e], Andrew Lee[b,c], Chad A. Mirkin[b,c,d,1], and Alexander H. Stegh[a,b,1]

[a]Ken and Ruth Davee Department of Neurology, The Northwestern Brain Tumor Institute, Robert H. Lurie Comprehensive Cancer Center, Northwestern University, Chicago, IL 60611; [b]International Institute for Nanotechnology, Northwestern University, Evanston, IL 60208; [c]Department of Chemistry, Northwestern University, Evanston, IL 60208; [d]Interdepartmental Biological Sciences Program, Northwestern University, Evanston, IL 60208; and [e]Department of Neurological Surgery, Northwestern University, Chicago, IL 60611

Contributed by Chad A. Mirkin, February 22, 2017 (sent for review September 13, 2016; reviewed by Robert Langer and Justin D. Lathia)

RNA interference (RNAi)-based gene regulation platforms have shown promise as a novel class of therapeutics for the precision treatment of cancer. Techniques in preclinical evaluation of RNAi-based nanoconjugates have yet to allow for optimization of their gene regulatory activity. We have developed spherical nucleic acids (SNAs) as a blood–brain barrier-/blood–tumor barrier-penetrating nanoconjugate to deliver small interfering (si) and micro (mi)RNAs to intracranial glioblastoma (GBM) tumor sites. To identify high-activity SNA conjugates and to determine optimal SNA treatment regimens, we developed a reporter xenograft model to evaluate SNA efficacy in vivo. Engrafted tumors stably coexpress optical reporters for luciferase and a near-infrared (NIR) fluorescent protein (iRFP670), with the latter fused to the DNA repair protein O^6-methylguanine-DNA-methyltransferase (MGMT). Using noninvasive imaging of animal subjects bearing reporter-modified intracranial xenografts, we quantitatively assessed MGMT knockdown by SNAs composed of MGMT-targeting siRNA duplexes (siMGMT-SNAs). We show that systemic administration of siMGMT-SNAs via single tail vein injection is capable of robust intratumoral MGMT protein knockdown in vivo, with persistent and SNA dose-dependent MGMT silencing confirmed by Western blotting of tumor tissue ex vivo. Analyses of SNA biodistribution and pharmacokinetics revealed rapid intratumoral uptake and significant intratumoral retention that increased the antitumor activity of coadministered temozolomide (TMZ). Our study demonstrates that dual noninvasive bioluminescence and NIR fluorescence imaging of cancer xenograft models represents a powerful in vivo strategy to identify RNAi-based nanotherapeutics with potent gene silencing activity and will inform additional preclinical and clinical investigations of these constructs.

spherical nucleic acid nanoconjugates | glioblastoma multiforme | O^6-methylguanine-DNA-methyltransferase | near-infrared fluorescence | bioluminescence

Functional cancer genomics has identified novel cancer-relevant genes as contributors to disease progression, and in so doing enabled the implementation of precision cancer medicine into clinical practice (1). Several targeted small molecule inhibitors and biotherapeutic antibodies have been FDA-approved, in particular those targeting a cancer cell's kinome. The majority of cancer genes, however, represent nonenzymatic targets with unknown mechanisms of action that cooperate to drive cancer progression and therapy resistance (1). To target "undruggable" gene products, RNAi-based nanoconjugates have been developed to robustly and safely deliver small interfering (si)RNA oligonucleotide payloads to tumor sites. However, in comparison with small molecule therapeutics, the development of RNAi-based nanotechnological platforms involves minimal optimization of conjugate chemistry and behavior on cellular and organismal levels. The difficulty in preparing, scaling, physicochemically characterizing, and functionally evaluating well-defined nanomaterials, together with the challenges in altering their structures in a modular fashion, have posed significant limitations on the in-depth characterization and optimization of nanomaterials. In addition, many nanoconstructs that elicit potent gene silencing activity in vitro, when administered systemically in animal subjects, are ineffective in treating tumors in vivo, mainly due to serum factors, renal filtration, liver modification, and limited ability to traverse biological barriers (2). To enable more meaningful preclinical in vivo evaluation of RNAi-based nanoconjugates, animal models need to accurately predict and confirm functionality of the intended constructs, as well as be rigorously used for the optimization of their administration and dosing schedule. Such effort would not only enable the therapeutic use of RNAi-based nanomaterials but would also aid in establishing these platforms as tools for discovery science. Nanoconjugates can be delivered to cells and animals without the need of auxiliary transfection agents or viruses. Furthermore, to study a gene's role in cancer progression, these nanoconjugates do not require lengthy optimization protocols or the

Significance

Small interfering (si) and micro (mi)RNA-carrying nanomaterials emerged as a new class of anticancer therapeutics. To enable quantification of intratumoral gene expression in response to RNAi nanoconjugate treatment in vivo, we developed a dual reporter glioblastoma xenograft model using cell lines that stably coexpress optical reporters for luciferase and a near-infrared fluorescent protein (iRFP670). We generated orthotopic glioblastoma multiforme tumors expressing an iRFP670-O^6-methylguanine-DNA-methyltransferase (MGMT) fusion protein for real-time assessment of MGMT-targeting spherical nucleic acids (i.e., gold-based nanoconjugates functionalized with siRNA oligonucleotides targeted to MGMT). We demonstrate that dual noninvasive bioluminescence and fluorescence imaging can determine intratumoral protein expression in response to systemic spherical nucleic acid treatment and represents an in vivo testing platform to facilitate preclinical investigations of nanoscale gene silencing therapeutics.

Author contributions: T.L.S., F.M.K., C.D.J., C.A.M., and A.H.S. designed research; T.L.S., F.M.K., L.A.H., T.J.M., A.C., J.L.M., S.T.G., L.E.C., T.C.C., S.N.B., A.J.S., N.S., and A.L. performed research; T.L.S., F.M.K., L.A.H., T.J.M., A.C., J.L.M., S.T.G., L.E.C., T.C.C., S.N.B., A.J.S., N.S., C.D.J., A.L., C.A.M., and A.H.S. analyzed data; and T.L.S., F.M.K., and A.H.S. wrote the paper.

Reviewers: R.L., Massachusetts Institute of Technology; and J.D.L., Cleveland Clinic.

Conflict of interest statement: C.A.M. has financial interests in/relative to AuraSense, LLC, and Exicure, Inc., which could potentially benefit from the outcomes of this research. A.H.S. has financial interests in/relative to Exicure, Inc., which could potentially benefit from the outcomes of this research.

[1]To whom correspondence may be addressed. Email: chadnano@northwestern.edu or a-stegh@northwestern.edu.

This article contains supporting information online at www.pnas.org/lookup/suppl/doi:10.1073/pnas.1702736114/-/DCSupplemental.

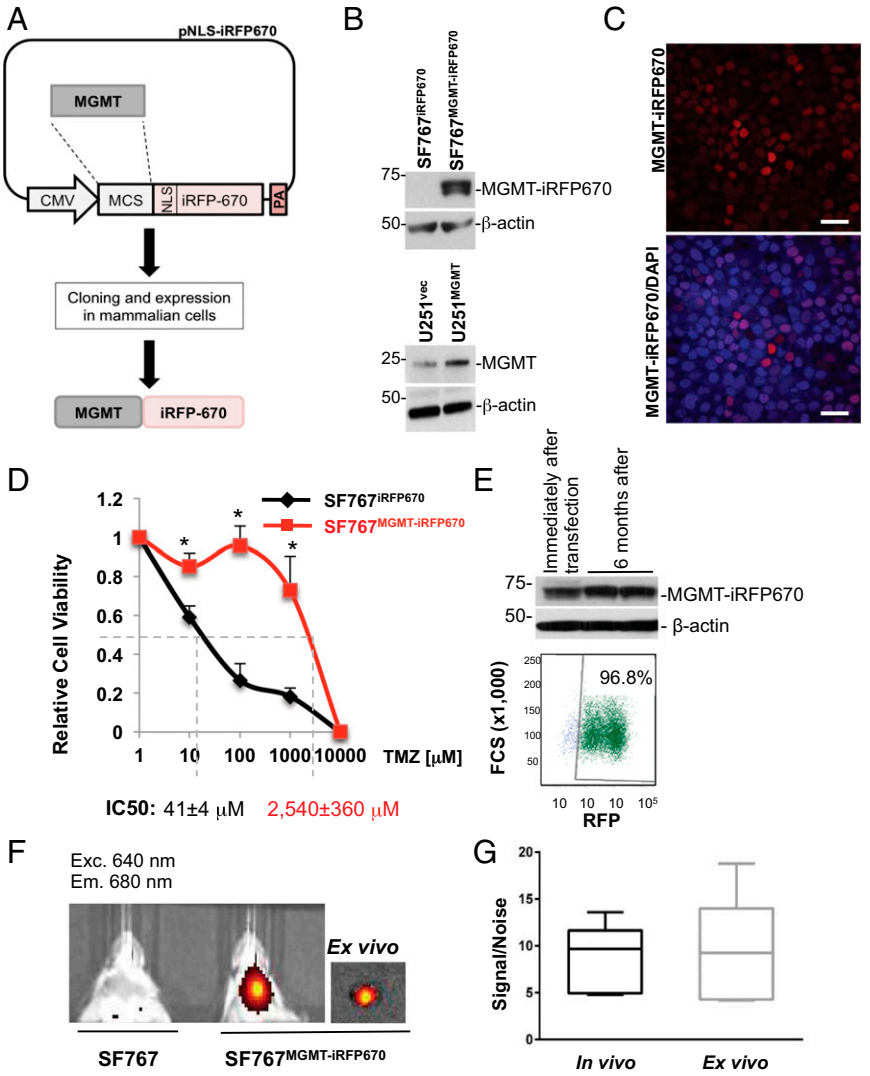

Fig. 1. Generation of MGMT-iRFP670–expressing cells and derivative orthotopic grafts. (*A*) Schematic of the expression plasmid encoding the MGMT-iRFP670 fusion product. (*B*) Western blot of MGMT expression from U251, U251^{MGMT}, SF767, and SF767$^{MGMT\text{-}iRFP670}$ cells. (*C*) Confocal microscopy images of SF767$^{MGMT\text{-}iRFP670}$ cells. (Scale bars, 30 μm.) (*D*) Cell viability analysis of SF767 and SF767$^{MGMT\text{-}iRFP670}$ cells to determine dose–response to TMZ. *$P < 0.05$. (*E*) Western blot analysis of MGMT expression from SF767$^{MGMT\text{-}iRFP670}$ cells immediately after selection of MGMT-iRFP670–expressing cells and 6 mo later. (*F*) IVIS imaging of SCID mice bearing SF767 and SF767$^{MGMT\text{-}iRFP670}$ cell orthotopic xenografts. (*G*) Box plot of signal-to-noise analysis of SF767$^{MGMT\text{-}iRFP670}$/ SF767 xenografts.

generation of cells modified for stable knockdown or knockout of the gene using CRISPR/Cas9 genome editing.

We have developed spherical nucleic acids (SNAs), which consist of a gold nanoparticle core densely functionalized with a shell of radially oriented siRNA oligonucleotides, to knock down gene expression in glioblastoma (GBM). GBM is an incurable brain cancer, with one of the poorest survival rates of 14–16 mo after diagnosis for patients that have undergone maximum surgical resection and subsequent radiation and temozolomide (TMZ) treatment (3–5). In contrast to free siRNA oligonucleotides, SNAs robustly enter almost all known cell lines, including patient-derived glioma cell cultures (GICs), effectively reducing gene expression (4, 5). In an in vitro blood–brain barrier (BBB) model involving the coculture of human primary brain microvascular endothelial cells separated from astrocytes by a semipermeable filter insert, SNAs rapidly traversed this biological barrier, passing through endothelial cells and the filter to enter the astrocytes (4). In vivo, SNAs crossed the BBB/blood–tumor barrier (BTB) upon systemic, i.v. administration to animal subjects bearing intracranial GBM tumors. Due to the enhanced permeability and retention effect (i.e., the ability of nanoconugates to preferentially accumulate in tumor vs. normal tissue), SNAs showed enhanced infiltration into GBM tumor compared with normal brain elements (4, 5). When functionalized with siRNA targeted to glioma oncogenes [i.e., the caspase and p53 inhibitor Bcl2Like12 (Bcl2L12)] (4), or with tumor-suppressive micro (mi)RNAs (i.e., miR-182) (5), SNAs triggered robust intratumoral target gene knockdown and impaired tumorigenicity (6).

In the current study we have developed intracranial xenograft models of GBM modified for stable expression of luciferase and a near-infrared (NIR) fluorescent protein fused to O^6-methylguanine-DNA-methyltransferase (MGMT). This model enables longitudinal and noninvasive determination of MGMT gene knockdown in response to the treatment with MGMT-specific SNAs in vivo. Leveraging this model system, we optimized SNAs carrying siRNA specific for MGMT in animal subjects in vivo to determine the most therapeutically effective siMGMT-SNA regimen, as monotherapy and in combination with TMZ. MGMT removes the cytostasis- and apoptosis-inducing methyl adducts added by TMZ, which impair the effectiveness of TMZ chemotherapy (7). Lower expression of MGMT protein has been linked to prolonged survival in GBM patients treated with alkylating agents, including TMZ, such as shown in the study by Lechapt-Zalcman et al. (8). In that study, patients with low levels of intratumoral MGMT protein were determined as surviving significantly longer from TMZ therapy relative to patients whose tumors expressed high levels of MGMT (27.0 mo vs. 15.1 mo posttreatment).

Results

Generation of MGMT-iRFP670-Expressing Cells and Derivative Orthotopic Grafts. To develop a GBM xenograft model capable of tracking MGMT expression in vivo, we generated an MGMT-iRFP670 expression construct by cloning the *MGMT* coding sequence in frame

with the NIR protein iRFP670 (Fig. 1*A*). Upon lipoplex-mediated transfection of the pNLS-MGMT-iRFP plasmid, cells were selected with G418 for 7 d and subsequently sorted for an iRFP-expressing cell population by FACS. Cellular expression of the MGMT-iRFP670 fusion was evaluated by Western blotting (Fig. 1*B*) and by confocal microscopy (Fig. 1*C*). We functionally confirmed SNA activity, using cell viability assays, which demonstrated that cells expressing the fusion protein but not control cells harboring iRFP670 protein only were less susceptible to TMZ treatment (Fig. 1*D*). Reporter expression was highly stable; Western blotting and flow cytometry analyses revealed that MGMT-iRFP670 protein levels were similar in cells lysed immediately after selection compared with cells that had been in culture for 6 mo without selection pressure, with 97% of cells positive for fusion protein expression (Fig. 1*E*). Importantly, in vivo imaging system (IVIS) analysis of intracranial xenografts confirmed MGMT-iRFP670 fusion protein expression in vivo and in excised tumors ex vivo (Fig. 1*F*), with specific NIR significantly above noise signal (Fig. 1*G*).

Generation of SNA Conjugates to Silence MGMT Expression. To generate MGMT-targeting spherical nucleic acids (siMGMT-SNAs) for in vitro as well as in vivo knockdown of MGMT, 13-nm gold nanoparticles were functionalized with propylthiolated, *MGMT*-targeting siRNA and backfilled with PEG, using a previously reported production approach (3–5) (Fig. 2*A*). The ability of these constructs to silence endogenous MGMT and ectopically expressed MGMT-iRFP670 in vitro was evaluated by Western blotting and confocal microscopy with quantification of fluorescence intensity showing >70% suppression of MGMT proteins in patient-derived GICs, transformed glioma (U251 and U87MG), and cervical carcinoma cells (SF767) (Figs. 2 *B–E*). We next examined proapoptotic caspase activation in GBM cells treated with siMGMT-SNAs in combination with TMZ and found that the use of siMGMT-SNAs in combination with TMZ consistently increased caspase activation, in relation to TMZ treatment plus nontargeting control SNAs (siCo-SNAs) alone (Fig. 2*F*). Lymphoma and melanoma cell line expression of endogenous MGMT was also examined for response to siMGMT-SNA treatments, with associated results supporting the knockdown effect and the increase in TMZ-induced caspase activity as being generalizable across different types of cancer (Figs. 2 *G–K*).

siMGMT-SNAs Silence MGMT Expression in Vivo. Our previous studies using both siRNA- and miRNA-based SNAs (4, 5) demonstrated robust BBB/BTB penetration and significant intracranial accumulation and retention. To analyze siMGMT-SNA nanoconjugate biodistribution and pharmacokinetic profiles, mice bearing intracranial xenografts were administered a single injection of siMGMT-SNAs then sacrificed at predetermined time points; their organs were harvested and analyzed by inductively coupled plasma mass spectrometry (ICP-MS) for gold accumulation. Results from this analysis revealed that siMGMT-SNAs have a distribution half-life of ~16 min (*SI Appendix*, Fig. S1 *A* and *B*) and distribute throughout all major organs, with greatest accumulation/retention in the liver and spleen. Importantly, intracranial retention was significant and persistent, with up to 8×10^{12} gold nanoparticles per gram of tissue or 1% of injected dose detectable during the 7-d course of analysis (*SI Appendix*, Fig. S1*C*).

To evaluate in vivo MGMT knockdown using siMGMT-SNAs, MGMT-iRFP670 and luciferase-modified GBM (U87MG) and cervical carcinoma (SF767) cells were orthotopically injected into SCID-NOD mice to model primary and metastatic brain cancer growth, respectively. Upon indication of tumor progression, established by fluorescence and bioluminescence monitoring,

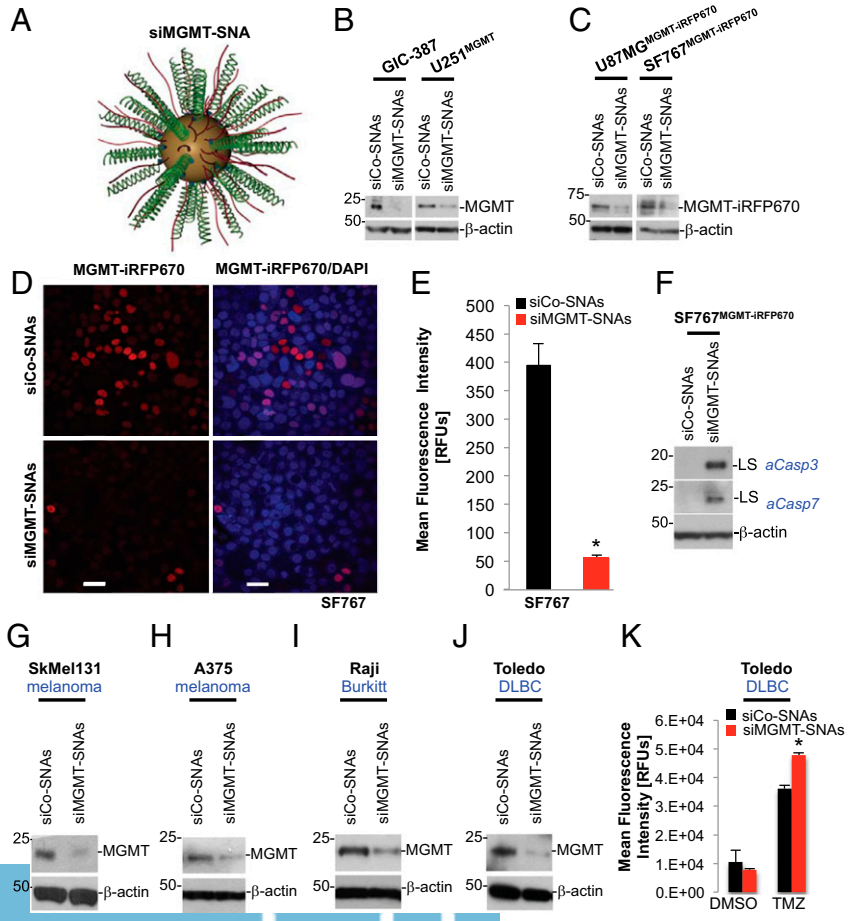

Fig. 2. siMGMT-SNAs silence MGMT and MGMT-iRFP670 expression and promote effector caspase-3 and -7 activation in conjunction with TMZ. (*A*) Schematic depicting siMGMT-SNAs. Green strands represent MGMT siRNA duplexes. Red strands represent PEG. (*B*) Western blot of MGMT expression from GIC-387 and U251^{MGMT} cells treated with either siCo-SNAs or siMGMT-SNAs. (*C*) Western blot of MGMT-iRFP670 from U87MG$^{MGMT\text{-}iRFP670}$ and SF767$^{MGMT\text{-}iRFP670}$ cells treated with siCo-SNAs or siMGMT-SNAs. (*D*) Confocal microscopy images of SF767$^{MGMT\text{-}iRFP670}$ cells treated with siCo-SNAs and siMGMT-SNAs. (Scale bars, 30 μm.) (*E*) Quantification of mean fluorescence intensity from confocal microscopy images of SF767$^{MGMT\text{-}iRFP670}$ cells treated with siCo-SNAs and siMGMT-SNAs (n = 10 images per SNA; *$P < 0.0001$). (*F*) Western blot of cleaved caspase-3 and -7 from U87MG$^{MGMT\text{-}iRFP670}$ cells treated with TMZ and either siCo-SNAs or siMGMT-SNAs. (*G–J*) siMGMT-SNAs silence endogenous MGMT expression in melanoma and lymphoma cell lines. Western blotting of MGMT expression in SkMel131 (melanoma), A375 (melanoma), Raji (Burkitt's lymphoma), and Toledo (diffuse large B-cell lymphoma) cell lines. (*K*) DEVDase assay of TMZ- and SNA-cotreated Toledo cells. *$P < 0.05$. siCo/siMGMT-SNAs, small interfering Control/MGMT spherical nucleic acids.

mice were administered with siMGMT-SNAs by tail vein injection (typically around 4 wk after tumor cell inoculation). Tumor luminescence and fluorescence values were obtained 24 h subsequent to treatment and compared against pretreatment readings. Relative MGMT protein knockdown was assessed by comparing the fluorescence to luminescence ratios of siMGMT-SNA–treated to siCo-SNA–treated mice. As shown in Fig. 3*A*, a single injection of siMGMT-SNAs was sufficient for achieving substantial knockdown of MGMT in vivo (Fig. 3*A*), and at levels comparable to knockdown achieved in vitro. MGMT knockdown was durable for up to 48 h after siMGMT-SNA injection (Fig. 3*B*). Following final in vivo imaging, mice were sacrificed and tumors resected for determination of intratumoral MGMT protein expression by Western blotting (Fig. 3 *C* and *D*), and for quantification of bioluminescence/fluorescence (Fig. 3*E*). Fig. 3*E* shows bioluminescence and fluorescence images of intracranial tumors that were used for tumor lysate preparation to assess MGMT-iRFP670 expression by Western blotting (shown in Fig. 3*D*). These data, together with detailed longitudinal assessment of MGMT fusion protein knockdown by IVIS in vivo (*SI Appendix*, Fig. S2*A*), ex vivo (*SI Appendix*, Fig. S2*B*), and by Western blotting of corresponding tumor cell lysate (*SI Appendix*, Fig. S2*C*), demonstrate significant correlation between reporter activity and Western blot signal.

siMGMT-SNAs Enhance TMZ Antitumor Effect in a Dose-Dependent Manner. To demonstrate the ability of our reporter model to accurately predict the most effective SNA treatment regimen, we treated mice bearing MGMT-iRFP670–expressing xenografts with three SNA doses, administered via a single i.v. injection (0.7, 1.4, or 2.8 mg/kg; dose based upon siRNA oligonucleotide concentration). As shown in Fig. 4 *A* and *B*, mice treated with 0.7 mg/kg experienced up to 26% MGMT protein knockdown. Two doublings of the single-administration amount (i.e., 1.4 and 2.8 mg/kg) increased MGMT knockdown to 59% and 72%, respectively. Guided by the collective results presented above, we injected siMGMT-SNAs at a dose of 1.4 mg/kg every 48 h to analyze the ability of the nanoconjugates to enhance TMZ antitumor effect. We chose the intermediate dosage because the treatment with higher SNA concentration did not lead to a statistically significant increase in knockdown efficacy. For this, mice received four i.v. siMGMT-SNA administrations on days 7, 9, 11, and 13 after tumor-cell injection, with TMZ administered daily at 66 mg/kg on days 8–12 (Fig. 4*C*). At all time points subsequent to initiation of treatment, mice treated with siMGMT-SNAs and

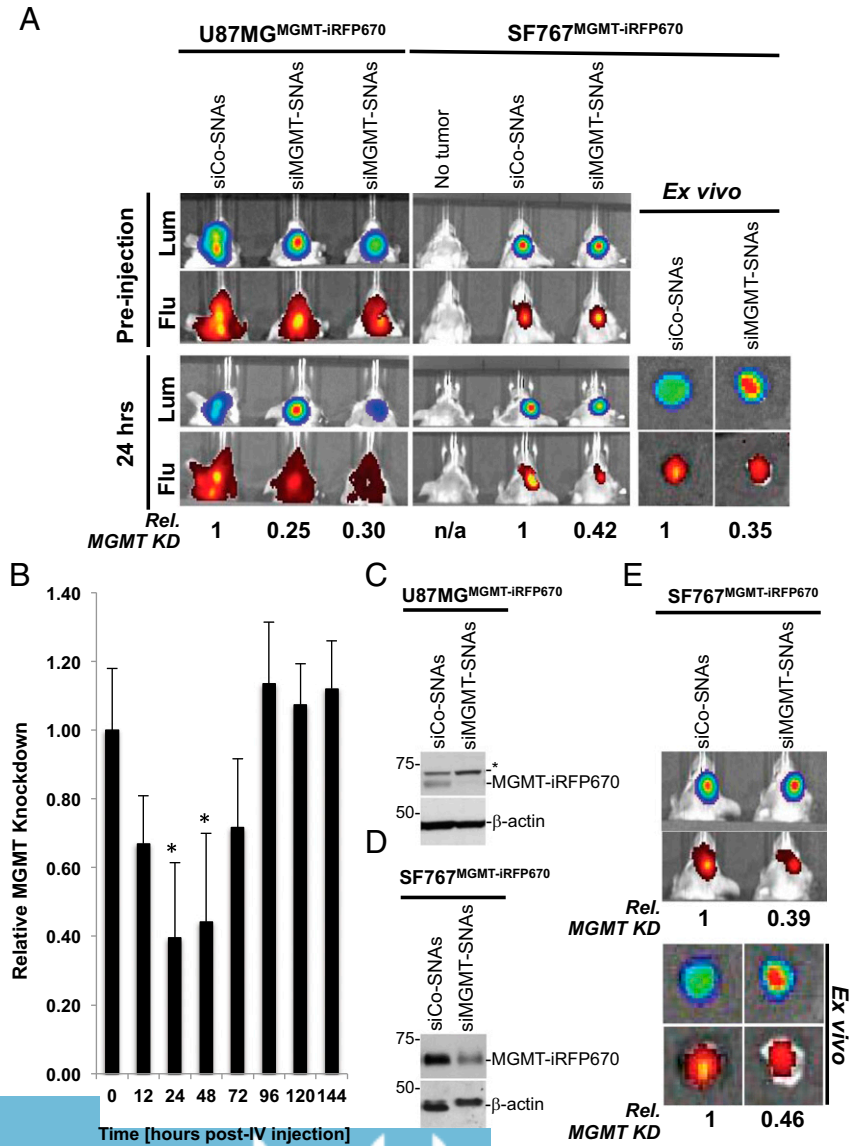

Fig. 3. siMGMT-SNAs silence MGMT-iRFP670 expression in intracranial xenografts. (*A*) (*Left*) Fluorescence (Flu) and luminescence (Lum) images of mice bearing U87MG$^{MGMT\text{-}iRFP670}$ xenografts before and 24 h after injection with siCo-SNAs or siMGMT-SNAs (1.4 mg/kg). (*Right*) Flu and Lum images of mice bearing SF767$^{MGMT\text{-}iRFP670}$ xenografts before and 24 h after injection with siCo-SNAs or siMGMT-SNAs. n/a, not applicable. (*B*) Longitudinal assessment of relative MGMT expression in intracranial tumors in response to siMGMT-SNA treatment. Asterisk indicates $P < 0.02$ for difference between relative MGMT expression at 0-h time point compared with 24- and 48-h time points (n = 8–28 mice per time point). (*C* and *D*) Western blot of MGMT-iRFP670 in U87MG$^{MGMT\text{-}iRFP670}$ and SF767$^{MGMT\text{-}iRFP670}$ tumor lysates 48 h after injection with siCo-SNAs or siMGMT-SNAs. (*E*) Flu and Lum images of mice bearing SF767$^{MGMT\text{-}iRFP670}$ xenografts, injected with siCo-SNAs or siMGMT-SNAs and imaged 48 h later; mice and tumors imaged were used for preparation of tumor cell lysates shown in *D*.

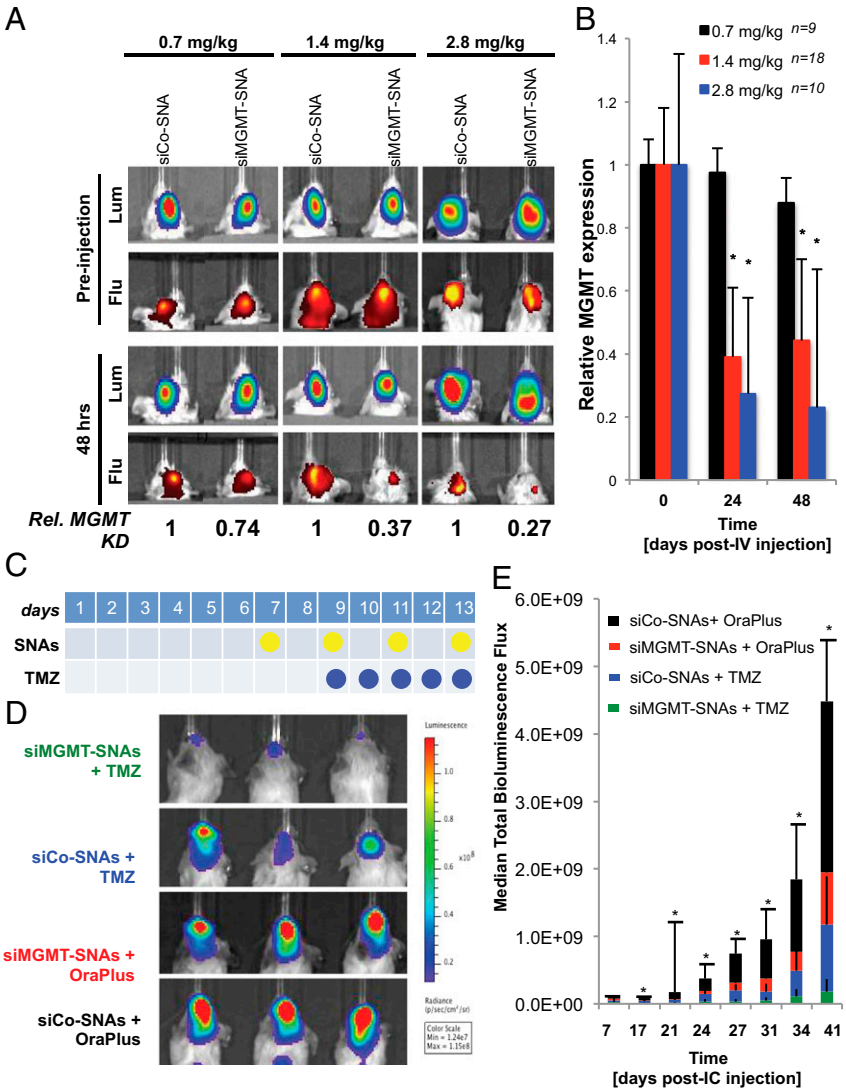

Fig. 4. Dose-dependent silencing of MGMT-iRFP670 expression with siMGMT-SNAs in intracranial xenografts. (*A*) Fluorescence and luminescence images of mice bearing SF767$^{MGMT\text{-}iRFP670}$ xenografts 48 h after injection with 0.7, 1.4, or 2.8 mg/kg siCo-SNAs or siMGMT-SNAs. (*B*) Kinetic assessment of dose-dependent silencing of MGMT-iRFP670 expression. Asterisk indicates $P < 0.05$ for the difference between the relative MGMT expression at the 0-h time point compared with 24- and 48-h time points ($n = 9$–18 mice per dose). (*C*) Schematic of SNA and TMZ dosing schedule. (*D*) Representative luminescence images of mice bearing GIC-20^{MGMT} xenografts treated with siCo-SNAs or siMGMT-SNAs and TMZ or OraPlus 41 d after intracranial injection of xenografts. (*E*) Median total bioluminescence flux from all treatment groups with time. Asterisk indicates $P < 0.02$ for bioluminescence difference between siMGMT-SNA+TMZ and siCo-SNA+TMZ groups ($n = 9$–10 mice per treatment group).

TMZ showed the lowest tumor luminescence values (Fig. 4 *D* and *E*), with a significant difference between siCo-SNA plus TMZ treatment vs. siMGMT-SNA plus TMZ treatment, evident at day 41 after tumor-cell injection (Fig. 4*E*; median total flux of 9.93×10^8 p/s vs. 1.82×10^8 p/s, $P < 0.03$).

Discussion

For this investigation, we created xenograft models expressing luciferase and an NIR fluorescent fusion protein (MGMT-iRFP670) to evaluate siRNA-based SNAs specific for MGMT. We used this model system to develop optimized SNA treatment regimens for the treatment of GBM engraftment models in vivo. Whereas NIR probes have been used in imaging application of brain tissue and exploited in preclinical molecular imaging studies (e.g., ref. 9), our study used NIR proteins as a tool to visualize and quantify the expression of oncoproteins in tumor tissue in real time. We used this model to demonstrate robust in vivo MGMT gene silencing capacity in intracranial tumors following intravascular administration of siMGMT-SNAs. MGMT silencing, in turn, significantly enhanced the antitumor activity of systemically administered TMZ. Significant advances in optimizing siRNA-based nanotherapeutics have been made in recent years (10, 11), and the clinical use of this class of therapeutics is now a reality (12). Increasing application of siRNA nanotherapeutics requires the development of relevant preclinical models for evaluating target knockdown, as well as the biologic effects of target knockdown, to test and identify administration regimens appropriate for clinical translation. Toward this goal, as concerns the treatment of GBM we have developed a dual bioluminescence/NIR fluorescence model to monitor tumor volume and intratumoral expression of the TMZ resistance factor MGMT. Bioluminescence monitoring, by labeling xenografts with luciferase, is an accurate method to assess tumor burden and provides a more reliable measurement of small or inaccessible tumors (i.e., intracranial GBM xenografts) than traditional caliper-based measurements (13, 14). For fluorescence monitoring in vivo, Verkhusha and coworkers (15) engineered NIR fluorescent proteins from bacterial phytochrome receptors, enabling rapid, inexpensive fluorescence detection and quantification. These NIR proteins were modified in spectra to allow for multicolor imaging and have since proven useful for fluorescence imaging-based tracking of primary and metastatic tumor tissue in vivo, and for flow cytometry-based quantification of fluorescence intensities in tumor cell subpopulations ex vivo (16–19). Relative to other imaging modalities, such as MRI, PET, and single-photon emission computed tomography this imaging technique is simple and comparatively high-throughput and does not require reporter probes, contrasting agents, or expensive imaging equipment (20).

Although applied to a specific tumor-therapeutic hypothesis here, our reporter knockdown approach should prove generalizable for evaluating, in medium throughput, knockdown efficacies of various RNAi-based nanoconjugates to target a broad spectrum of

oncogenic and therapy resistance factors. Because SNAs are modular structures (21), particle size, shape, and surface chemistry can be individually and independently controlled, making it possible to create large numbers of structurally defined and functionally distinct particles, which subsequently can be enrolled into an in-depth in vivo evaluation of gene silencing activity.

Materials and Methods

Mammalian Plasmids and Transfection Conditions. To monitor MGMT expression in vivo, an MGMT fusion protein was constructed using the NIR fluorescent protein iRFP670 (34 kDa, excitation/emission maxima at 640 nm/680 nm), using the pNLS-iRFP670 plasmid (16). The *MGMT* gene was PCR-amplified using specific primers (forward: GCGCAAGCTTCCATGCTGGGACAGCCCGC, reverse: GCGCGAATTCGTTTCGGCCAGCAGGCGGG) and cloned into the pNLS-iRFP670 plasmid vector using HindIII and EcoRI (NEB) restriction sites. Next, the cells were transfected using Lipofectamine 2000 (Invitrogen) with pNLS-MGMT-iRFP670 according to manufacturer's protocol. The culture media were changed to fresh DMEM containing 10% (vol/vol) FBS 24 h posttransfection. Stably expressing cells were selected using G418 antibiotic. Positive cells were sorted using FACS analysis (Beckman Coulter). To stably overexpress nontagged MGMT protein, 5 μL of Lenti-GIII-CMV-MGMT-GFP-2A-Puro (ABM, Inc.) were added to 75% confluent U251 cells or GIC-20 at 1×10^6 cells per T-25 flask for 48 h, followed by FACS analysis to enrich for GFP-positive cells.

Luciferase Expression. Tumor cells (U87MG and GIC-20) were transduced with a lentiviral construct containing the *firefly luciferase* (*fluc*) gene under the control of a spleen focus-forming virus promoter. Lentiviruses were generated by the cotransfection of 293T cells with three plasmids (gag, pol, env, and fluc). Forty-eight hours after transfection, supernatant with virus was collected and passed through a 22-μm filter. The filtered supernatant was used to infect the target cells, with transduced cells established as intracranial tumors in immunodeficient mice.

siMGMT-SNA and siCo-SNA Synthesis. Citrate-stabilized gold nanoparticles (AuNPs, 13 ± 1 nm) were prepared using the Frens method (22), treated with 0.1% diethylpyrocarbonate (Sigma-Aldrich), and autoclaved. RNA duplexes (MGMT siRNA duplex: sense strand GAUGGAUGUUUGAGCGACAdTdT(Sp18)$_2$SH, antisense strand UGUCGCUCAAACAUCCAUCdTdT; control siRNA duplex: sense strand CUUACGCUGAGUACUUCGAdTdT(Sp18)$_2$SH, antisense strand UCGAAGUACUCAGCGUAAGdTdT) were hybridized and added to RNase-free AuNPs containing 150 mM NaCl and 0.2% Tween-20 at a ratio of 2 nmol RNA duplex per 1 mL AuNP. To shield the electrostatic repulsion around the RNA duplexes and improve RNA loading on the AuNPs, the NaCl concentration was increased to 350 mM over 4 h. RNA-coated AuNPs were then treated with 20 μM mPEG-SH (2 kDa; Laysan Bio, Inc.) for 72 h, purified by transflow filtration (50-kDa mPES filters; Spectrum Laboratories, Inc.), and suspended in sterile, RNase-free PBS to the desired concentration for the intended application.

Tumor Xenograft Model and in Vivo SNA and TMZ Administration. All animals used were under an approved protocol of the Institutional Animal Care and Use Committee of Northwestern University. For intracranial cell inoculation, U87MG$^{MGMT\text{-}iRFP670}$, SF767$^{MGMT\text{-}iRFP670}$ cells or GIC-20^{MGMT} were suspended in Hank's balanced salt solution at a concentration of 5×10^5, 5×10^5, and 3×10^5 per 3 μL, respectively. Anesthetized female CB17 SCID mice (6–8 wk) (Taconic Farms) were placed in a stereotaxic frame, and the surgical area was cleaned with Betadine. An incision was made, and a 0.7-mm burr hole was created in the skull with a microsurgical drill, 2 mm lateral right of the sagittal suture and 0.5 mm posterior of bregma. Cells were administered through a Hamilton syringe, which was inserted 3 mm into the brain. Cells were injected over a period of 3 min. To demonstrate MGMT knockdown efficacy of SNAs, siMGMT- or siCo-SNAs were administered through the tail vein and the knockdown effects were measured by IVIS imaging at different time points posttreatment. To demonstrate therapeutic efficacy of siMGMT-SNAs as a monotherapy and in combination with TMZ, 500 nM of siMGMT- or siCo-SNAs were administered via the tail vein at the indicated doses [antisense RNA (milligrams) per mouse weight (kilograms)] per injection. TMZ was suspended in OraPlus (Paddock Laboratories) at a concentration of 10 mg/mL administered by oral gavage at a dose of 66 mg/kg for five consecutive days starting 1 d after the first SNA injection. To measure the signal-to-noise ratio, the fluorescence/bioluminescence signal of mice bearing glioma orthotopic xenografts expressing both luciferase and MGMT-iRFP670 was compared with the fluorescence/bioluminescence signal of non-tumor-bearing mice.

ACKNOWLEDGMENTS. This research was supported by the Center for Cancer Nanotechnology Excellence initiative of the NIH under Award U54 CA151880 (to A.H.S. and C.A.M.), National Institute of Arthritis and Musculoskeletal and Skin Diseases Award R01AR060810 (to C.A.M.), Defense Advanced Research Projects Agency Grant HR0011-13-2-0018 (to C.A.M.), the John McNicholas Foundation and the American Cancer Society (A.H.S.), National Cancer Institute/NIH National Research Service Award Fellowship F30CA174058-01 (to T.L.S.), a Ryan Fellowship (T.L.S. and J.L.M.), a National Science Foundation graduate research fellowship and a P.E.O. scholar award (S.N.B.), the Northwestern University Flow Cytometry Facility, Northwestern University Center for Advanced Microscopy, and Cancer Center Support Grant NCI CA060553.

1. Stegh AH (2013) Toward personalized cancer nanomedicine - past, present, and future. *Integr Biol* 5(1):48–65.
2. Whitehead KA, et al. (2012) In vitro-in vivo translation of lipid nanoparticles for hepatocellular siRNA delivery. *ACS Nano* 6(8):6922–6929.
3. Giljohann DA, Seferos DS, Prigodich AE, Patel PC, Mirkin CA (2009) Gene regulation with polyvalent siRNA-nanoparticle conjugates. *J Am Chem Soc* 131(6):2072–2073.
4. Jensen SA, et al. (2013) Spherical nucleic acid nanoparticle conjugates as an RNAi-based therapy for glioblastoma. *Sci Transl Med* 5(209):209ra152.
5. Kouri FM, et al. (2015) miR-182 integrates apoptosis, growth, and differentiation programs in glioblastoma. *Genes Dev* 29(7):732–745.
6. Mirkin CA, Stegh AH (2014) Spherical nucleic acids for precision medicine. *Oncotarget* 5(1):9–10.
7. Sharma S, et al. (2009) Role of MGMT in tumor development, progression, diagnosis, treatment and prognosis. *Anticancer Res* 29(10):3759–3768.
8. Lechapt-Zalcman E, et al. (2012) O(6) -methylguanine-DNA methyltransferase (MGMT) promoter methylation and low MGMT-encoded protein expression as prognostic markers in glioblastoma patients treated with biodegradable carmustine wafer implants after initial surgery followed by radiotherapy with concomitant and adjuvant temozolomide. *Cancer* 118(18):4545–4554.
9. Deliolanis NC, et al. (2014) Deep-tissue reporter-gene imaging with fluorescence and optoacoustic tomography: A performance overview. *Mol Imaging Biol* 16(5):652–660.
10. Akinc A, et al. (2008) A combinatorial library of lipid-like materials for delivery of RNAi therapeutics. *Nat Biotechnol* 26(5):561–569.
11. Alabi CA, et al. (2013) Multiparametric approach for the evaluation of lipid nanoparticles for siRNA delivery. *Proc Natl Acad Sci USA* 110(32):12881–12886.
12. Lytton-Jean AK, Kauffman KJ, Kaczmarek JC, Langer R (2015) Cancer nanotherapeutics in clinical trials. *Cancer Treat Res* 166:293–322.
13. Dinca EB, et al. (2007) Bioluminescence monitoring of intracranial glioblastoma xenograft: Response to primary and salvage temozolomide therapy. *J Neurosurg* 107(3):610–616.
14. Ozawa T, James CD (2010) Establishing intracranial brain tumor xenografts with subsequent analysis of tumor growth and response to therapy using bioluminescence imaging. *J Vis Exp* 2010(41), 10.3791/1986.
15. Filonov GS, et al. (2011) Bright and stable near-infrared fluorescent protein for in vivo imaging. *Nat Biotechnol* 29(8):757–761.
16. Shcherbakova DM, Verkhusha VV (2013) Near-infrared fluorescent proteins for multicolor in vivo imaging. *Nat Methods* 10(8):751–754.
17. Piatkevich KD, Subach FV, Verkhusha VV (2013) Engineering of bacterial phytochromes for near-infrared imaging, sensing, and light-control in mammals. *Chem Soc Rev* 42(8):3441–3452.
18. Zdobnova T, et al. (2015) A novel far-red fluorescent xenograft model of ovarian carcinoma for preclinical evaluation of HER2-targeted immunotoxins. *Oncotarget* 6(31):30919–30928.
19. Telford WG, Shcherbakova DM, Buschke D, Hawley TS, Verkhusha VV (2015) Multiparametric flow cytometry using near-infrared fluorescent proteins engineered from bacterial phytochromes. *PLoS One* 10(3):e0122342.
20. Weissleder R (2002) Scaling down imaging: Molecular mapping of cancer in mice. *Nat Rev Cancer* 2(1):11–18.
21. Rouge JL, et al. (2015) Ribozyme-spherical nucleic acids. *J Am Chem Soc* 137(33):10528–10531.
22. Frens G (1973) Controlled nucleation for the regulation of the particle size in monodisperse gold suspensions. *Nat Phys Sci (Lond)* 241:20–22.